Supporting Information for

A one-demand solar hydrogen-evolution system for unassisted high-efficiency pure water splitting

Wei Che,[1] Hui Su,[1] Xu Zhao,[1] Yuanli Li,[1,2] Hui Zhang,[1] Wanlin Zhou,[1] Meihuan Liu,[1] Weiren Cheng,[1] Fengchun Hu,[1] and Qinghua Liu[1,*]

[1]*National Synchrotron Radiation Laboratory, University of Science and Technology of China, Hefei 230029, Anhui, P. R. China*

[2]*Fundamental Science on Nuclear Wasters and Environmental Safety Laboratory, Southwest University of Science and Technology, Mianyang 621010, Sichuan, P. R. China*

S1. Synthetic strategy.

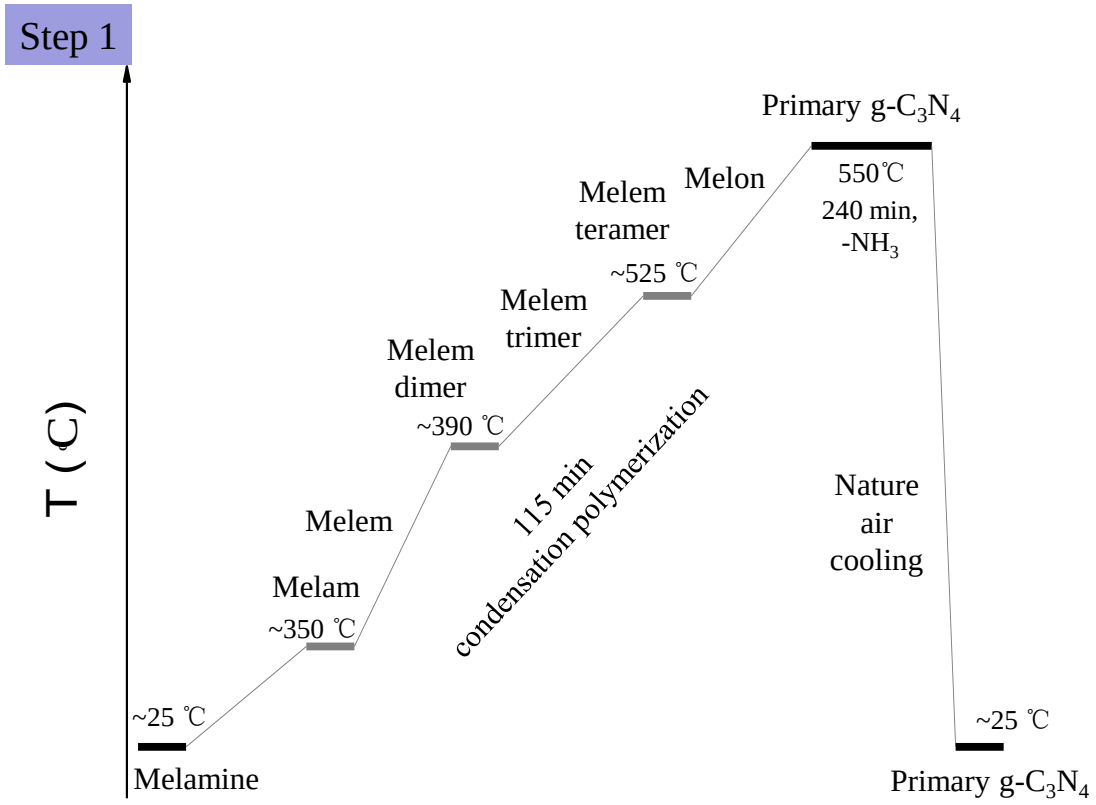

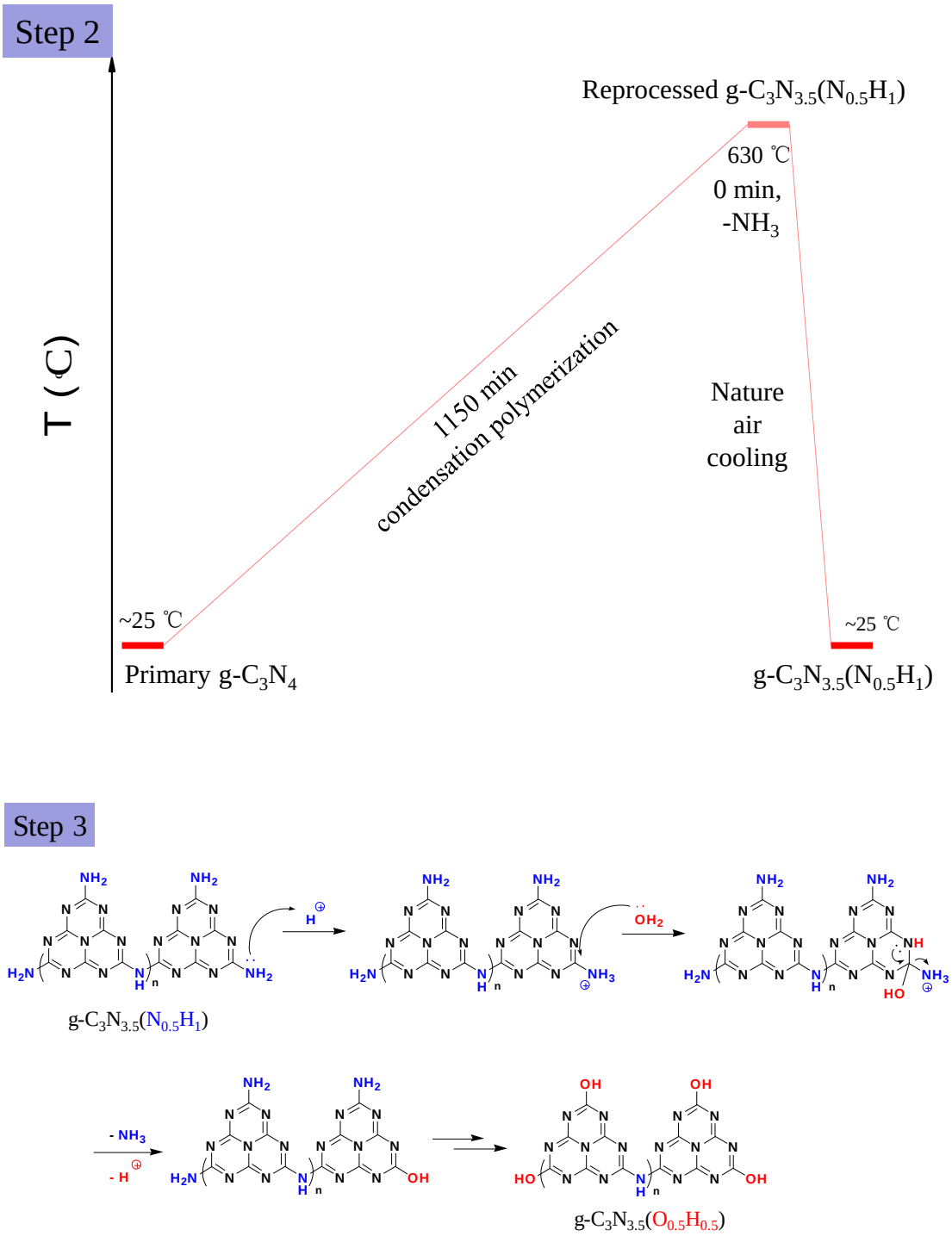

Figure S1. The thermal polymerization procedures of step 1 to produce pristine g-C_3N_4; The transformation from g-C_3N_4 to "-NH_2" featured g-$C_3N_{3.5}(N_{0.5}H_1)$ by step 2; The conversion mechanism of g-$C_3N_{3.5}(O_{0.5}H_{0.5})$ terminal groups from -NH_2 to -OH in step 3.

S2. Materials characterization.

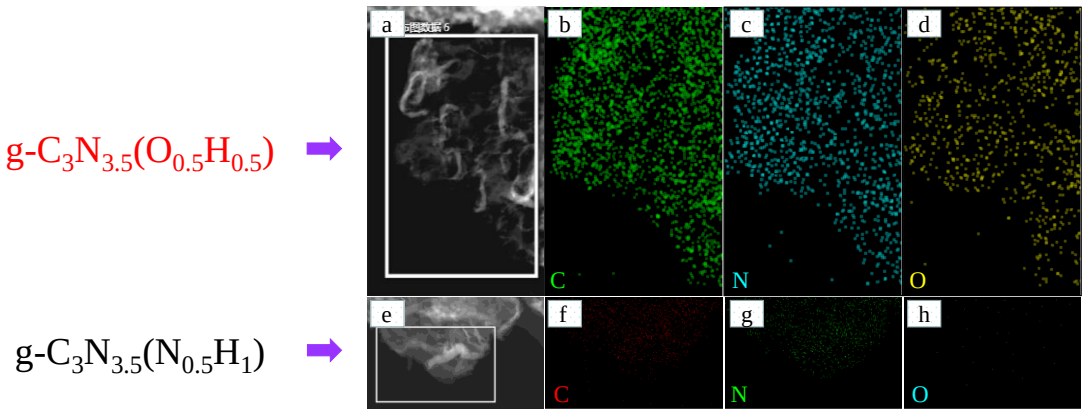

Figure S2. TEM-EDS mapping images.

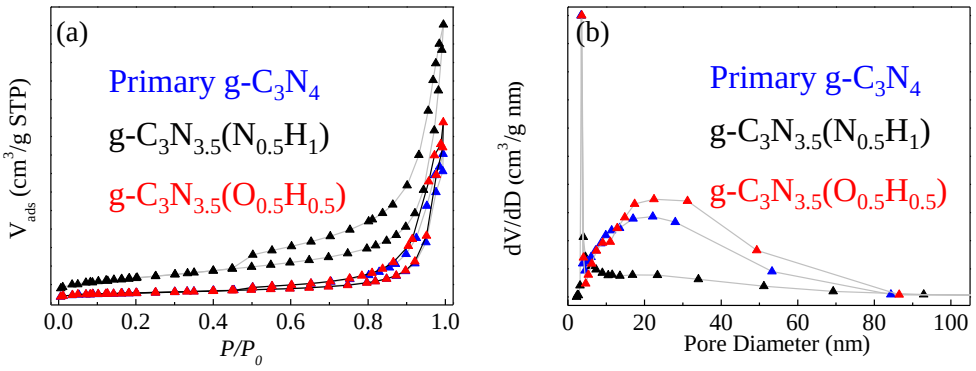

Figure S3. Pore volumes from the BET isotherms.

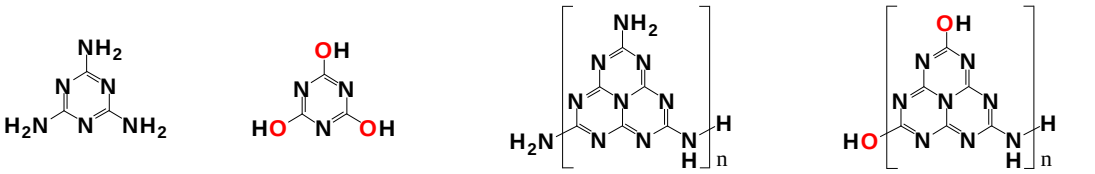

Figure S4. The corresponding formula of guide samples.

XANES measurements. The C and N *K*-edge X-ray absorption near-edge spectra (XANES) were measured at BL12B-a beamline of National Synchrotron Radiation Laboratory (NSRL, China) in the total electron yield (TEY) mode by collecting the sample drain current under a vacuum better than 5×10^{-8} Pa.[1,2] The beam from the bending magnet was monochromatized utilizing a varied linespacing plane grating and refocused by a toroidal mirror. The energy range is 100–1000 eV with an energy resolution of ca. 0.2 eV. For the XANES measurement, incident X-ray beam with high energy resolution of 0.1 eV were used. During the XANES measurement, the samples were firmly adhered on the conductive substrate with random orientation, so the polarization dependence is not considered here.

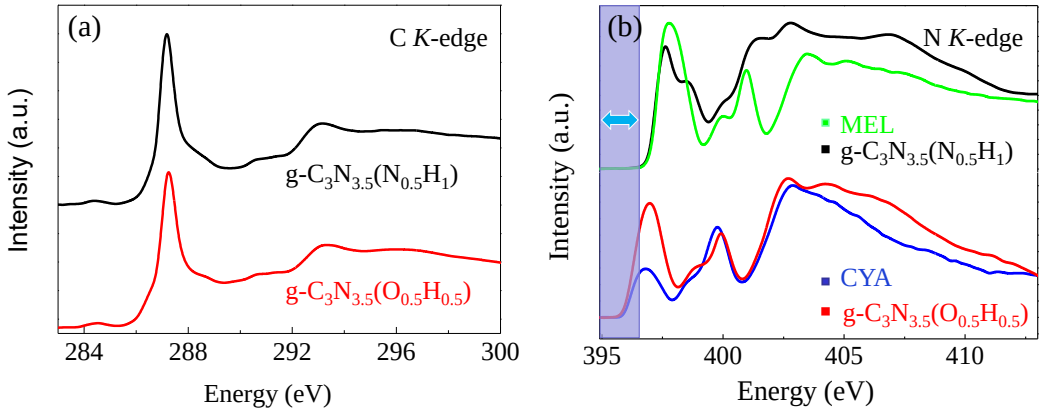

Figure S5. (a) C K-edge X-ray absorption near edge structure spectroscopy of g-$C_3N_{3.5}(N_{0.5}H_1)$ and g-$C_3N_{3.5}(O_{0.5}H_{0.5})$; (b) N K-edge X-ray absorption near edge structure spectroscopy for MEL, CYA , g-$C_3N_{3.5}(N_{0.5}H_1)$ and g-$C_3N_{3.5}(O_{0.5}H_{0.5})$.

The curves of g-$C_3N_{3.5}(N_{0.5}H_1)$ and g-$C_3N_{3.5}(O_{0.5}H_{0.5})$ in XANES C 1s spectra, show almost identical characteristic peaks, offering the information that the materials under homologous conditions share the same tri-s-triazine unit derived from the graphitic p-conjugated stacking structure.[1] Coming from a similar nitrogen environment of tri-s-triazine member, the N 1s spectra of g-$C_3N_{3.5}(N_{0.5}H_1)$ and g-$C_3N_{3.5}(O_{0.5}H_{0.5})$ are almost identical for peak shape, which have three sharp peaks a, b, c and a broad peak d. Distinctly, there is the difference in initial position that peak position of

g-$C_3N_{3.5}(N_{0.5}H_1)$ and g-$C_3N_{3.5}(O_{0.5}H_{0.5})$ are have a difference of 1 eV.[3] Compared to g-$C_3N_{3.5}(N_{0.5}H_1)$, the shapes of the two spectral peaks are almost identical, which have shown three sharp peaks a, b, and c at the energies of 396.5, 398.4, and 399.7 eV and a broad peak d.[4]

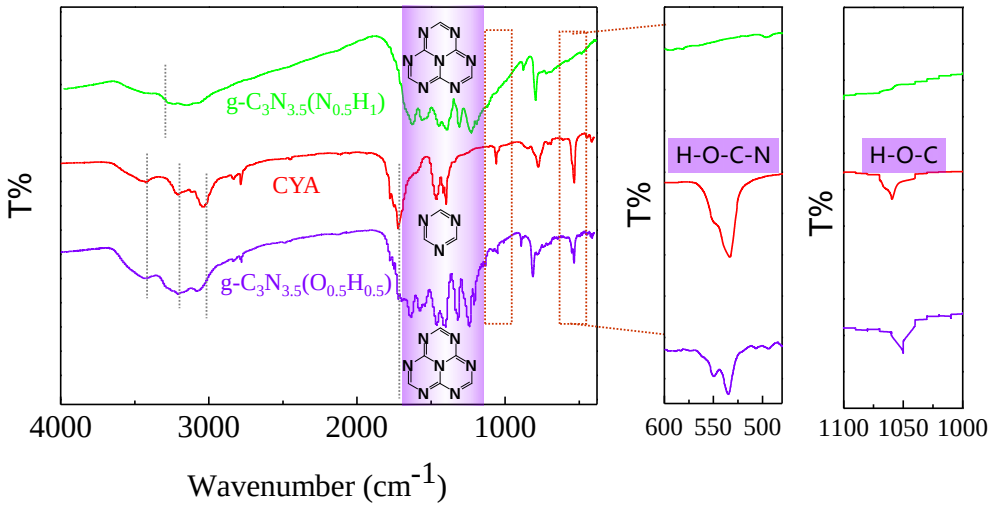

Figure S6. FT-IR and the magnified FT-IR spectra.

The typical stretching mode of C-N heterocycles in the 1200–1600 cm^{-1} region and the breathing mode of the heptazine units at 800 cm^{-1} are found in g-$C_3N_{3.5}(O_{0.5}H_{0.5})$, indicating that the formation of extended C-N-C networks of g-C_3N_4 almost maintains after the terminal chemical modification. The symmetric and antisymmetric -NH_2 stretching modes of g-C_3N_4 are found in the high-frequency region at approximately 3300cm^{-1}.[5] As for g-$C_3N_{3.5}(O_{0.5}H_{0.5})$, the new band at about 1750 cm^{-1} was attributed to C=O stretching. There are three characteristic bands at 3000–3600 cm^{-1} can be ascribed to the stretching modes of O–H resulted from Cyanuric acid. The existence of intermolecular hydrogen bond formation can lower the O–H stretching frequency. In addition, the strong band at 540 cm^{-1} and 1050 cm^{-1} found in the g-$C_3N_{3.5}(O_{0.5}H_{0.5})$ and cyanuric acid correspond to H-O-C-N and C-O-H in-plane bending vibrations showing that the existence plenty of hydroxyl groups on the g-C_3N_4 after the terminal chemical modification.[6]

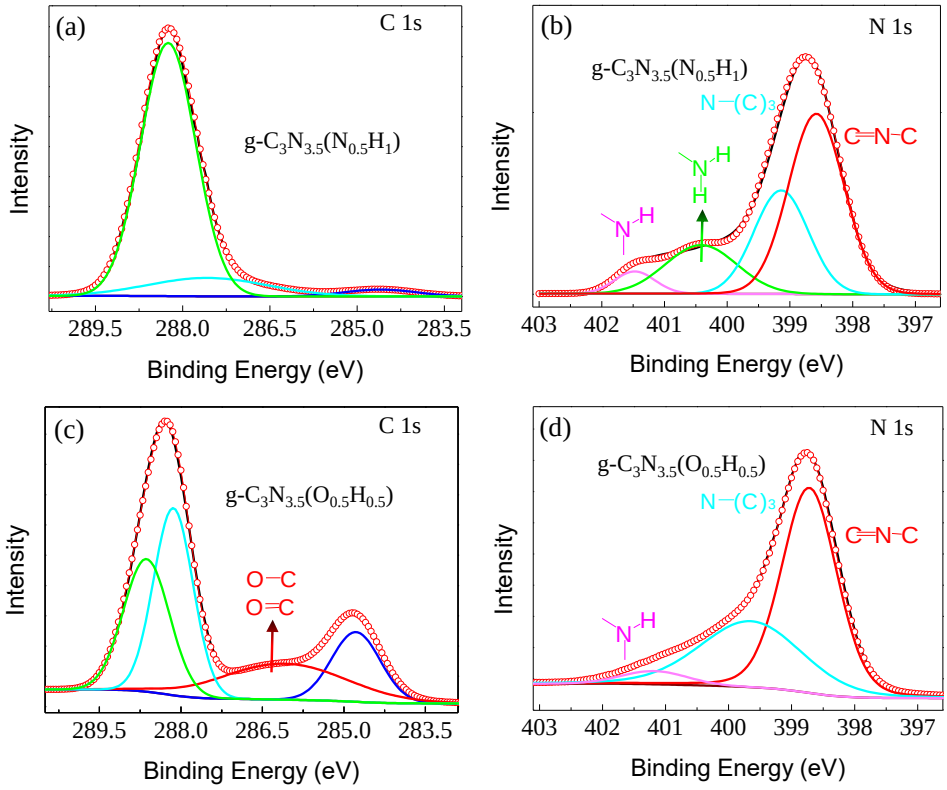

Figure S7. XPS spectra for the samples.

The surface chemical composition was investigated by X-ray photoelectron spectroscopy (XPS). The peak fittings were performed using the Casa XPS software. The background correction was performed using a Shirley background. The spectra were fitted with Peak shapes modeled using Gaussian Laurentzian profile. XPS spectrum is used to further investigate environment and chemical environment of g-$C_3N_{3.5}(N_{0.5}H_1)$ and g-$C_3N_{3.5}(O_{0.5}H_{0.5})$. For pure g-$C_3N_{3.5}(N_{0.5}H_1)$, C 1s shows peaks at 288.3 eV, 287.9 e V and 284.6 eV was assigned to sp2-hybridized C-N in triazine, C bonded to three N atoms inside the triazine structures and defect C-C bonds coupling in the triazine units respectively.[7] g-$C_3N_{3.5}(O_{0.5}H_{0.5})$ shows high content of C-C bonds at 284.6 eV. It is worth noting that the XPS peak with binding energy of 286.3 eV has been attributed to O species of C-O and C=O, giving the strong evidence of classical melem-OH structure for g-$C_3N_{3.5}(O_{0.5}H_{0.5})$. The formation interaction of N species is also investigated in high resolution N 1s XPS spectra. The N 1s spectrum shows the different contents of nitrogen environments in binding

energies at about 398.5 eV, 399.1 eV, 400.3 eV and 401.5 eV, where the peaks can be indexed to sp^2 hybridized C-N=C, tertiary N (N-$(C)_3$) groups and amino functional groups (C-N-H), respectively. Moreover, the disappearance of peak at about 400.3 eV confirmed the removed -NH_2 groups at the interface π-conjugate g-$C_3N_{3.5}(O_{0.5}H_{0.5})$.[3,8]

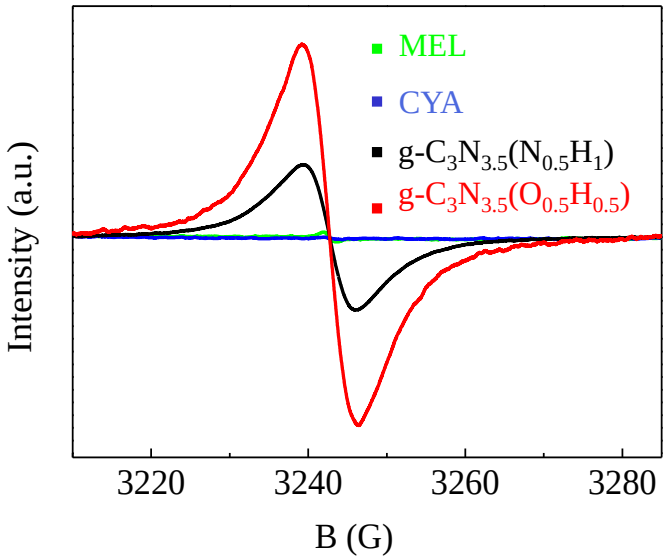

Figure S8. EPR spectra for the samples.

A Lorentzian line centering at a g value of 2.0034 can be observed, which can be ascribed to the generation of unpaired electrons on aromatic rings. The EPR signals of MEL and CYA are rather weak. For g-$C_3N_{3.5}(N_{0.5}H_1)$ and g-$C_3N_{3.5}(O_{0.5}H_{0.5})$ samples, the intensity of Lorentzian lines increases with π bonded nanosized oligomers. The Lorentzian line in g-$C_3N_{3.5}(N_{0.5}H_1)$ has been greatly enhanced after replacing the defects "-NH_2" with "-OH". Thus, the formation of the " melem-OH" can help to optimize the electronic structure for charge migration and separation.[9]

Photocatalytic activity. The photocatalytic overall water-splitting reactions were carried out in a top-irradiation type photoreactor (Pyrex glass) connected to a closed gas circulation system.[10] Typically, 30 mg of the photocatalysts were dispersed in 100 ml pure water in 100 mL and the deposition of ~2 wt % Pt cocatalyst was conducted by directly dissolving trace $H_2PtCl_6.6H_2O$ into the above 100 mL reaction solution.

The reaction solution was evacuated several times to remove air completely, and then irradiated by a 300 W Xe-lamp (PLS-SXE 300, Beijing perfectlight Co. Ltd, China). Therefore, the evolved hydrogen and oxygen can be measured by a gas chromatograph (GC) equipped with a thermal conduction detector (TCD, 5 Å molecular sieve columns with 3 m length) using Ar as carrier gas with flow rate of 20 ml/min. Photocatalytic test method is consistent with the standard measurement with the most previous reports. The 30 cycles with time interval of 6 hours were performed. The quantum efficiency (QE) was estimated by the method from equation as follows[11]:

$$QE\,(\%) = \frac{2 \times H}{I} \times 100$$

H and I represent the numbers of evolved H_2 molecules and incident photons. Several band-pass filters of full width at half maximum (FWHM)=15 nm were employed under a 300 W Xe lamp for measurement of the quantum efficiency. The average intensity of each irradiation wavelength was determined by an optical power meter (PM100D, Thermal Powermeter Head, THORLABS). For full spectrum (λ>300 nm) measurement, a 300 W xenon arc lamp (PLS-SXE300/300UV) with a standard AM1.5 filter was used as irradiation light source.

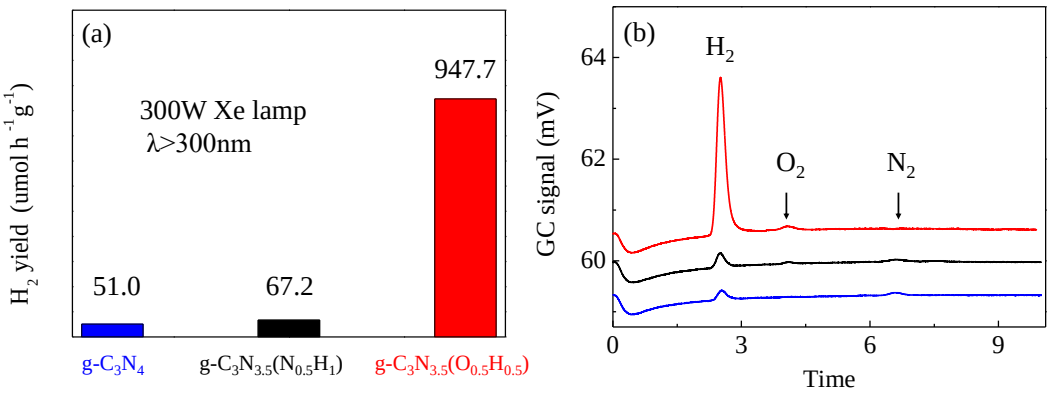

Figure S9. (a) Photocatalytic activity in pure water: prestine g-C_3N_4 (blue), reprocessed g-$C_3N_{3.5}(N_{0.5}H_1)$ (dark) and g-$C_3N_{3.5}(O_{0.5}H_{0.5})$ (red); (b) The reaction

system was evacuated after each run after 1 h light illumination. The on-line GC signals to quantify the H_2, O_2 and N_2 gases produced: prestine g-C_3N_4 (blue), reprocessed g-$C_3N_{3.5}(N_{0.5}H_1)$ (dark) and g-$C_3N_{3.5}(O_{0.5}H_{0.5})$ (red).

The H_2O_2 generation in OWS. The results presented in the Figure 4a using o-tolidine as the peroxide indicator: First, 2.0 mL reaction suspension for OWS that was taken immediately after the irradiation. Then, photocatalyst is removed from the solution by centrifugation immediately. 1 ml 1% o-tolidine in 1 M HCl was added to the suspension above without stirring. Allowed to react for 3 min, UV–vis absorption spectrum was used to characterize the solution. The typical peak of the 2-electron oxidized toluidine generated by H_2O_2 has a characteristic maximum at 438 nm.[12,13] The results presented in the Figure 4b: Under standard reaction and measurement conditions stated in the test of OWS. The experiments evaluated in pure water without any sacrificial reagents after irradiation in the powder suspension with a period of time. the produced gases of the reaction system was evacuated immediately. Then, the system was left in the dark for an hour, O_2 release from H_2O_2 was examined and No H_2 was detected. The results are presented in the Figure 4b. The results presented in the Figure 4c: A reference experiment was conducted to verify the rapid decomposition of H_2O_2 in the closed gas circulation system. An adscitious aqueous H_2O_2 solution in closed gas circulation system was evacuated several times to remove air completely. Then the evolved gas can be measured by a gas chromatograph (GC) equipped with a thermal conduction detector. The volume fraction of H_2O_2 and water is 0.005 (0.5ml/99.5ml).

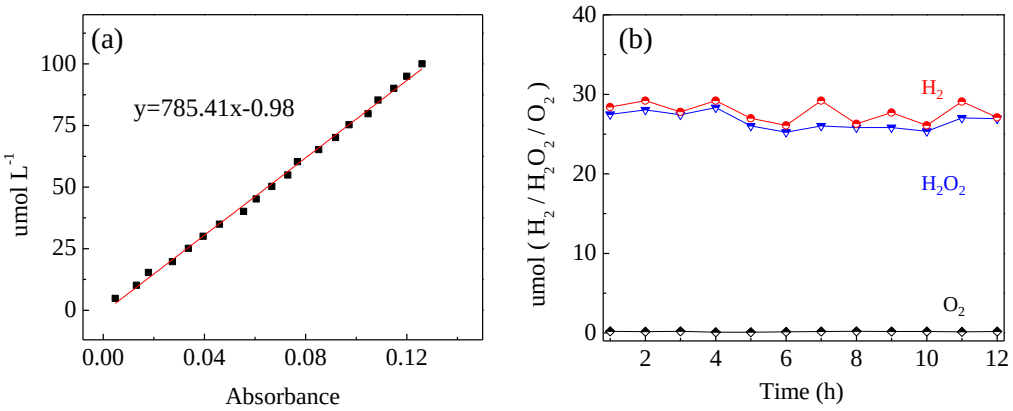

Figure S10. (a) The calibration curve and fitting equation of the absorbance and concerntration, which are determined by o-tolidine as the peroxide indicator; (b) Time resolved H_2、O_2 and H_2O_2 evolution data for hydroxylated g-$C_3N_{3.5}(O_{0.5}H_{0.5})$ photocatalyst directly performed in pure water.

The reaction system was evacuated after each run with 1 h light illumination. The on-line GC signals to quantify the H_2 and O_2 gases yield by g-$C_3N_{3.5}(O_{0.5}H_{0.5})$ have been cumulated by each hour. Simultaneously, the amount of H_2O_2 generated in the catalysts surface was detected by the detailed process: 1.0 ml reaction suspension for OWS that was taken immediately after the irradiation. Then, photocatalyst is removed from the solution by centrifugation immediately. 1 mL 1% o-tolidine and 1ml 0.1 M HCl was added to the suspension above without stirring. Allowed to react for 3 min, UV–vis absorption spectrum was used to characterize the absorbance of solution. As seen from Figure N3b, the time course of H_2O_2 from OWS shows the free H_2O_2 production in the reaction solution during 12 hours. The detection of H_2O_2 is calculated by the corresponding calibration curve in Figure S10a. With the increase of time, the amount of produced free H_2O_2 increases gradually. As expected, time course of H_2 and H_2O_2 production remains no noticeable decrease during the 12-hour test. O_2 evolution was inefficient under OWS measurement conditions due to the kinetic bottleneck for O_2 evolution via four-electron process in valence band. Compared the amount of H_2 produced in CB, the amount of H_2O_2, which were produced via two-electron pathway, nearly form in a 1:0.96 stoichiometry with H_2. The amounts of

missing H_2O_2 may come from very small amounts O_2 evolution or small amounts of coordinated peroxide in the catalyst surface. After 12-hour test, the observed H_2: H_2O_2 ratio (1:0.96) is in accordance with charge balance of the electrons and holes, which means that carriers involved in OWS are used efficiently.

Electrochemical measurement methods. Electrochemical measurements were performed using an electrochemical workstation (Model CHI760D, CH instruments, Inc., Austin, TX) with a standard three-electrode photoelectrochemical cell and was used to record transient photocurrent behavior of the samples, where the prepared electrodes immersed in a sodium sulfate electrolyte solution (0.5 M), a gauze platinum and Ag/AgCl (saturated KCl) act as the working, auxiliary, and reference electrode, respectively. The working electrodes were prepared as follows: Fluoride tin oxide (FTO) glass was washed sequentially with acetone, ethanol and DI water in an ultrasonic bath for 30 min. Next, 0.05 g of photocatalyst was ground with 5 uL nafion (5 wt%, Sigma Aldrich) and mixed with 2 mL of acetone under sonication for 30 min to obtain slurry. Then, the slurry was coated onto 1 cm × 2 cm FTO glass electrode by the spin coater. After air-drying, the electrodes were sintered at 350 ℃ for 120 min to improve adhesion. In addition, the three electrodes were immersed in a sodium sulfate electrolyte solution (0.5 M) as conductive media at pH 6.8, which was continuously in an N_2-purged flow to remove O_2 before light irradiation. Photocurrent measurements utilized a 300 W Xe lamp. The working electrode was back-illuminated through the FTO glass in order to minimize absorption by the dark and thick catalyst layer. Potential window of Mott-Schottky measurement for working electrodes was set to the ranged from -0.2 to 0.9V, and the perturbation signal was an AC voltage magnitude of 5 mV with the frequency at 1.5, 2 and 3 kHz. The electrochemical impedance spectroscopy (EIS) was measured at -0.4 V, and the perturbation signal was also 5 mV with the frequency ranged from 0.1 Hz to 100 kHz. The photoresponse of the prepared photoelectrodes (I-t) was operated by measuring the photocurrent densities under chopped light irradiation (light on/off cycles: 50s) at a bias potential of -0.4 V. The transient open-circuit voltage decay (OCVD) measurements were taken

for 800s in all, and the light on and off were controlled at 200s and 400s from the start, respectively. The average lifetime of the photogenerated carriers (τ_n) were obtained from the OCVD according to equation[14]:

$$\tau_n = -\frac{k_B T}{q}\left(\frac{dV_{OC}}{dt}\right)^{-1}$$

Where k_B is the Boltzmann constant, T is the temperature (in Kelvin), and q is the unsigned charge of an electron.

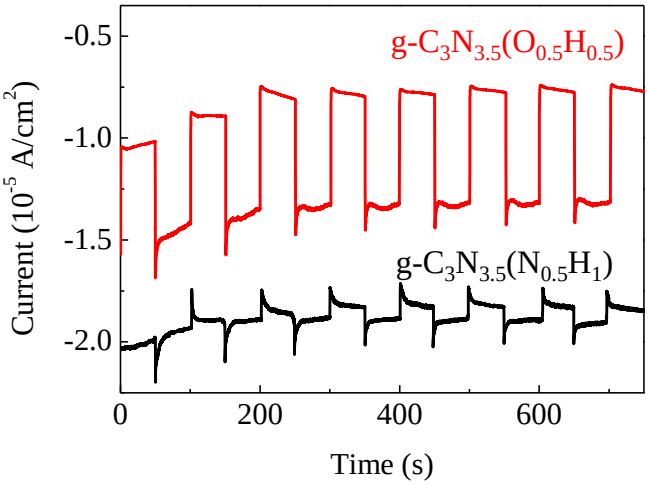

Figure S11. Photocurrent transient measurements.

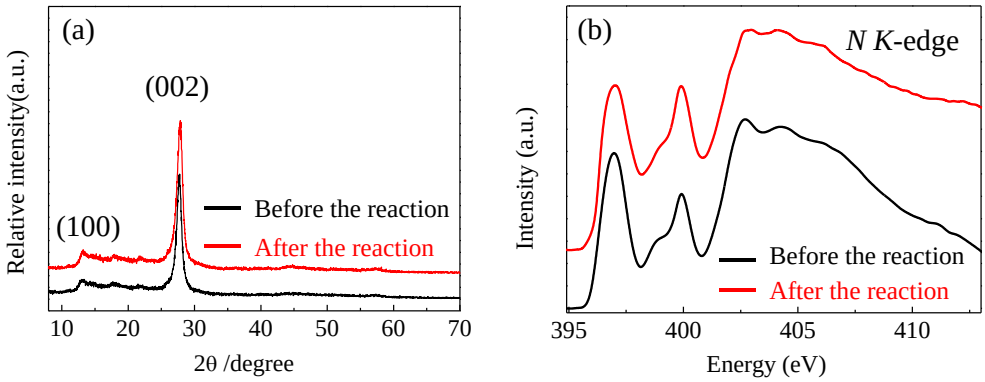

Figure S12. XRD and XANES measurements for g-$C_3N_{3.5}(O_{0.5}H_{0.5})$ before and after the photocatalytic activity test.

For comprehensive comparisons, the crystal phases of the hydroxylated g-$C_3N_{3.5}(O_{0.5}H_{0.5})$ photocatalyst before and after the photocatalytic activity test were analyzed by XRD and XANES characterization. The diffraction peak at (002) in Figure S12a confirmed the stable skeleton of the π–π stacking structure at interlayer distance of 3.20 Å. Peak (100) indicated that the fingerprints are repeated melem-based functional unit with a spacing of 6.91 Å, which implies that hydroxylated g-$C_3N_{3.5}(O_{0.5}H_{0.5})$ is an efficient and stable photocatalyst. Also, the stability of g-$C_3N_{3.5}(O_{0.5}H_{0.5})$ has been evaluated by XANES characterization which is highly sensitive to the interfacial environment. Based on the accordant results of in Figure S12b, it can be drawn that it is the hydroxylation of terraces/interfaces that effectively protect the photocatalyst from H_2O_2 poisoning.

Table S1. BET surface area and Elemental analysis.

Sample	$S_{BET}/(m^2/g)$	C wt %	N wt %	O wt %
Primary g-C_3N_4	33	49.15	50.39	0.46
g-$C_3N_{3.5}(N_{0.5}H_1)$	77	42.59	56.73	0.68
g-$C_3N3.5(O_{0.5}H_{0.5})$	94	40.04	46.52	13.44

Carbon nitride whose virtue of the incorporation of nitrogen atoms in the carbon structure can be easily synthesized by a typical thermopolymerization process. Previous publications generally depict g-C_3N_4 as an idealized 2D C-N polymer. But it is in fact that the the atomic composition ratio of carbon nitrides claiming "C_3N_4" does not equal to stoichiometric ratio 3 to 4. From XPS spectrum, the atomic C:N ratio for the as-produced primary g-C_3N_4 is 0.975, which is in accord with the previous reports.[15] In the second step of synthetic strategy, the atomic C:N ratio for produced g-CN material is 0.751. The substantially increasing range of N content indicates the local coordination environment of "melem-NH_2" at the boundary has been more fully exposed. In the third step of synthetic strategy, there are large

amounts of oxygen are present in g-$C_3N_{3.5}(O_{0.5}H_{0.5})$. The N content (C:N, 0.861) decreased significantly, due to replacement engineering from "–NH_2" to "–OH". Here, the carbon nitrides with the N wt% of 50.39 was denoted prestine g-C_3N_4 here. The reprocessed carbon nitrides with N wt% of 56.73 was termed g-$C_3N_{3.5}(N_{0.5}H_1)$, due to the increased range of N content in the second step of synthetic strategy is equal to the proportion of 0.5/4: (56.73-50.39)/50.39=0.5/4. Thus, the oxygen-containing carbon nitrides produced in the hydrolytic process was refered as g-$C_3N_{3.5}(O_{0.5}H_{0.5})$.

Table S2. Recent advances in overall water-splitting in pure water are summarized in in the following sections.

Catalysts	Pure water (redox pair)	Mass (mg)	Incident light	Cocatalysts (Loading)	H_2 rate (umol h^{-1} g^{-1})	(Ref.)
g-C_3N_4	Pure water	200	300 W Xe lamp > 300 nm	3 wt % pt	61	[16]
PPy/g-C_3N_4	Pure water	100	300 W Xe lamp > 300 nm	3 wt % pt	156	[17]
g-C_3N_4/$BiVO_4$	Pure water	300	300 W Xe lamp > 395 nm	3 wt % pt	15	[18]
g-C_3N_4/WO_3	Pure water	300	300 W Xe lamp > 395 nm	3 wt % pt	74	[18]
TiO_2/C_3N_4 (1%Pt) -$Ni(OH)_2$/WO_3(PtOx)	Pure water (NaI)	200	150 W Xe lamp > 200 nm	1 wt % pt	250	[19]
TiO_2/g-C_3N_4-WO_3(1%PtOx)	Pure water ($FeCl_2$)	200	150 W Xe lamp > 200 nm	1 wt % pt	50.46	[19]
TiO_2/g-C_3N_4-$Ni(OH)_2$/WO_3	Pure water (NaI)	200	150 W Xe lamp > 200 nm	1 wt % pt	19.4	[19]
Pt–Co/g-C_3N_4	Pure water	200	300 W Xe lamp > 300 nm	3 wt % pt	61	[16]
C-dot/g-C_3N_4	Pure water	80	300 W Xe lamp > 420 nm	-	575	[13]
g-C_3N_4/MnO_2	Pure water	100	300 W Xe lamp > 420 nm	-	55.3	[20]
Pt-CoP/g-C_3N_4	PH=3	80	300 W Xe lamp > 400 nm	3 wt % pt 3 wt % CoP	26.25	[21]
Co1-phosphide/PCN	Pure water	20	300 W Xe lamp > 300 nm	-	410.3	[22]
Primary g-C_3N_4	Pure water	30	300 W Xe lamp > 300 nm	2 wt % pt	51.0	This work

g-$C_3N_{3.5}(N_{0.5}H_1)$	Pure water	30	300 W Xe lamp > 300 nm	2 wt % pt	67.2	This work
g-$C_3N3.5(O_{0.5}H_{0.5})$	Pure water	30	300 W Xe lamp > 300 nm	2 wt % pt	947.7	This work

S3. The formulas involved.

Ideal process in regard to the concerted four-electron pathways for overall water splitting:

$$H_2O \rightarrow \frac{1}{2}O_2 + H_2 \qquad \Delta G = 237\ kJ\ mol^{-1} \qquad (1)$$

Realistic processes occurred under potentials of semiconductor based water-splitting (CB< 0.00 eV, VB > 1.78 eV):

$$2H_2O \rightarrow H_2O_2 + 2H_2 \qquad (2)$$

$$H_2O_2 \rightarrow 1/2O_2 + H_2O \qquad \Delta G = -106.1\ kJ\ mol^{-1} \qquad (3)$$

The competing photo-reduced processes in CB:

$$2H^+ + 2e^- \rightarrow H_2 \quad (-OH\ group - do\min ated\ process) \qquad (4)$$

$$O_2 + H^+ + e^- \rightarrow HO_2^{\bullet} \quad (-NH_2\ group - do\min ated\ process\ 5-7) \qquad (5)$$

$$HO_2^{\bullet} + H^+ + e^- \rightarrow H_2O_2 \qquad +1.51\ eV \qquad (6)$$

$$O_2 + 2H^+ + 2e^- \rightarrow H_2O_2 \qquad +0.70\ eV \qquad (7)$$

$$O_2 + 4H^+ + 4e^- \rightarrow H_2O \qquad (8)$$

The competing processes in VB:

$$2H_2O \rightarrow 4H^+ + O_2 + 4e^- \qquad 1.23\ eV \qquad (9)$$

$$2H_2O \rightarrow H_2O_2 + 2H^+ + 2e^- \qquad 1.78\ eV \qquad (10)$$

References

1 S. S. Roy, R. McCann, P. Papakonstantinou, J. A. McLaughlin, I. W. Kirkman, S. Bhattacharyya and S. R. P. Silva, *J. Appl. Phys.*, 2006, **99**, 043511(1)-043511(5).

2 S. Bhattacharyya, M. Lübbe and F. Richter, *J. Appl. Phys.*, 2000, **88**, 5043–5049.

3 Y. Zheng, Y. Jiao, Y. Zhu, L. H. Li, Y. Han, Y. Chen, A. Du, M. Jaroniec and S. Z. Qiao, *Nat. Commun.*, 2014, **5**, 3783.

4 Shimoyama. I, G. Wu, T. Sekiguchi, Y. Baba, Phys. Rev. B, 2000, **62**, R6053–R6056.

5 G. Dołęga, G. Lipner, M. Antonietti, S. Blechert, L. Möhlmann, G. Zhang, X. Wang, S. Lin, J. Zhang and X. Chen, *Angew. Chemie Int. Ed.*, 2012, **51**, 3183–3187.

6 T. E. Chien, K. L. Li, P. Y. Lin and J. L. Lin, *Langmuir*, 2016, **32**, 5306–5313.

7 Y. Zhao, F. Zhao, X. Wang, C. Xu, Z. Zhang, G. Shi and L. Qu, *Angew. Chemie Int. Ed.*, 2014, **53**, 13934–13939.

8 T. Y. Ma, S. Dai, M. Jaroniec and S. Z. Qiao, *Angew. Chemie Int. Ed.*, 2014, **53**, 7281–7285.

9 S. Lin, X. Wang, M. Zhang, G. Zhang, X. Qiu and X. Ye, *Adv. Mater.*, 2013, **26**, 805–809.

10 W. Che, W. Cheng, T. Yao, F. Tang, W. Liu, H. Su, Y. Huang, Q. Liu, J. Liu, F. Hu, Z. Pan, Z. Sun and S. Wei, *J. Am. Chem. Soc.*, 2017, **139**, 3021–3026.

11 J. Hong, X. Xia, Y. Wang and R. Xu, *J. Mater. Chem.*, 2012, **22**, 15006–15012.

12 X. Wu, J. Zhao, S. Guo, L. Wang, W. Shi, H. Huang, Y. Liu and Z. Kang, *Nanoscale*, 2016, **8**, 17314–17321.

13 J. Liu, Y. Liu, N. Liu, Y. Han, X. Zhang, H. Huang, Y. Lifshitz, S. T. Lee, J. Zhong and Z. Kang, *Science*, 2015, **347**, 970–974.

14 S. Bai, L. Yang, C. Wang, Y. Lin, J. Lu, J. Jiang and Y. Xiong, *Angew. Chemie Int. Ed.*, 2015, **54**, 14810–14814.

15 V. W. H. Lau, I. Moudrakovski, T. Botari, S. Weinberger, M. B. Mesch, V. Duppel, J. Senker, V. Blum and B. V. Lotsch, *Nat. Commun.*, 2016, **7**, 12165.

16 G. Zhang, Z. A. Lan, L. Lin, S. Lin and X. Wang, *Chem. Sci.*, 2016, **7**, 3062–3066.

17 Y. Sui, J. Liu, Y. Zhang, X. Tian and W. Chen, *Nanoscale*, 2013, **5**, 9150–9155.

18 D. J. Martin, P. J. T. Reardon, S. J. A. Moniz and J. Tang, *J. Am. Chem. Soc.*, 2014, **136**, 12568–12571.

19 J. Yan, H. Wu, H. Chen, Y. Zhang, F. Zhang and S. F. Liu, *Appl. Catal. B Environ.*, 2016, **191**, 130–137.

20 J. Liu, N. Y. Liu, H. Li, L. P. Wang, X. Q. Wu, H. Huang, Y. Liu, F. Bao, Y. Lifshitz, S. T. Lee and Z. H. Kang, *Nanoscale*, 2016, **8**, 11956–11961.

21 Z. Pan, Y. Zheng, F. Guo, P. Niu and X. Wang, *ChemSusChem*, 2017, **10**, 87–90.

22 W. Liu, L. Cao, W. Cheng, Y. Cao, X. Liu, W. Zhang, X. Mou, L. Jin, X. Zheng, W. Che, Q. Liu, T. Yao and S. Wei, *Angew. Chemie Int. Ed.*, 2017, **56**, 9312–9317.